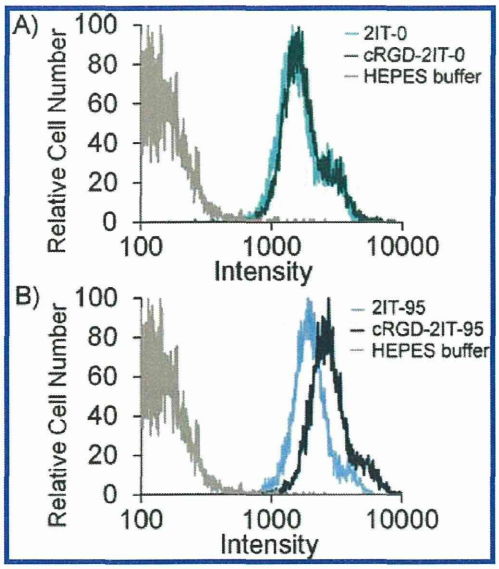

Figure 4. Cellular uptake of micelles in HeLa-luc cells. Cells were incubated with micelles prepared with fluorescent siRNA for 2 h (300 nM siRNA) prior to analysis by flow cytometry.

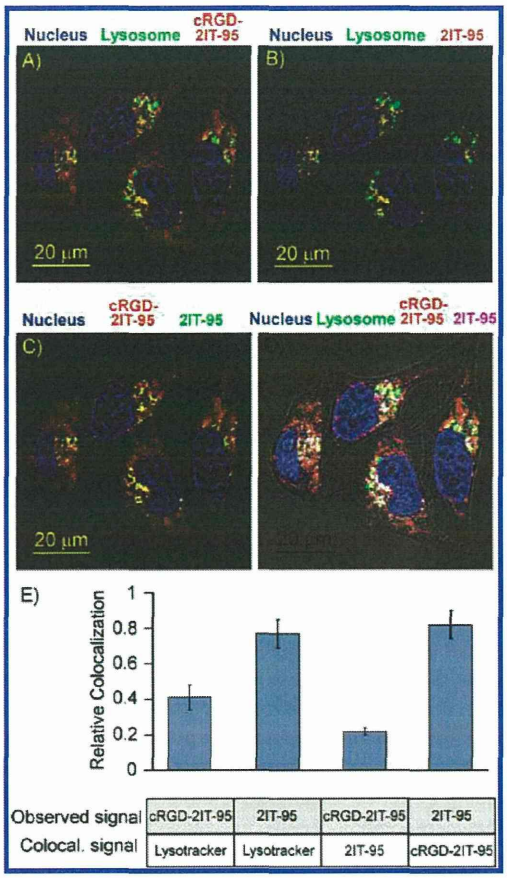

Figure 5. Subcellular distribution of 2IT-95 and cRGD-2IT-95 micelles following coincubation in HeLa-luc cells for 4 h (500 nM siRNA for each micelle formulation). Lysosomes were stained with LysoTracker green and micelles were prepared with Cy3- or Cy5-labeled siRNA for cRGD-2IT-95 and 2IT-95 formulations, respectively. (A–C) Cell images showing individual fluorescence signals. (D) Overlay of all fluorescent signals onto the transmitted image. (E) Quantification of fluorescence signal colocalization (n = 8 cells from two different images).

Increased cell uptake may be due to the ability of stable micelle structures to present multiple cRGD peptides on the nanoparticle surface. The presence of multiple cRGD peptides in close proximity has been shown to increase integrin binding efficiency in other studies.[29,30] Specifically, the binding constant of a cyclic decapeptide functionalized with cRGD increased 10-fold upon increasing the cRGD valency from one to four.[31] Similarly, a cRGD-functionalized PAMAM dendrimer showed a 100-fold increase in integrin binding affinity by increasing the number of cRGD peptides per dendrimer from one to eight.[32] Our results showing that stable micelle particles were needed to realize a benefit from cRGD targeting seems consistent with other reports that show more cRGD peptides in close proximity generally improves performance. However, in the case of the polymeric micelles described here, there seems to be a critical density of cRGD needed for improved performance to be realized.

In addition to improving cell uptake, the cRGD peptide may affect subcellular trafficking of attached cargo. Micelle structures (and generally macromolecules, as well) must be actively internalized into cells by endocytosis, which results in encapsulation within membrane-bound organelles (endosomes and lysosomes). We were specifically interested to see if the micelles used here were trafficked to lysosomes, as these subcellular vesicles can be a "dead end" for nucleic acids due to their function of degrading substances internalized within the cell.[33] Thus, we investigated the subcellular distribution of fluorescent-labeled siRNA contained within cRGD-2IT-95 or 2IT-95 micelles (samples that showed a difference in gene silencing ability and cell uptake). Lysosome compartments were stained with LysoTracker Green, which is specific marker for these acidic organelles. Micelle subcellular distribution was markedly different between the two formulations when co-incubated with HeLa-luc cells (Figure 5A–D). cRGD-2IT-95 micelles exhibited a broader cell distribution, and less than 50% of micelles were localized within lysosome compartments (Figure 5E), which is consistent with our previous report describing decreased lysosomal accumulation of pDNA polyplexes containing the cRGD peptide.[21] In contrast, 2IT-95 micelles were mostly confined to lysosome compartments (~80%). Further analysis of the fluorescent signals showed that cRGD-2IT-95 micelles were able to co-accumulate with 2IT-95 micelles within lysosomes, but 2IT-95 micelles were unable to colocalize with cRGD-2IT-95 micelles in nonlysosomal regions (Figure 5E). This result demonstrates that the cRGD peptide affects the subcellular fate of micelles,

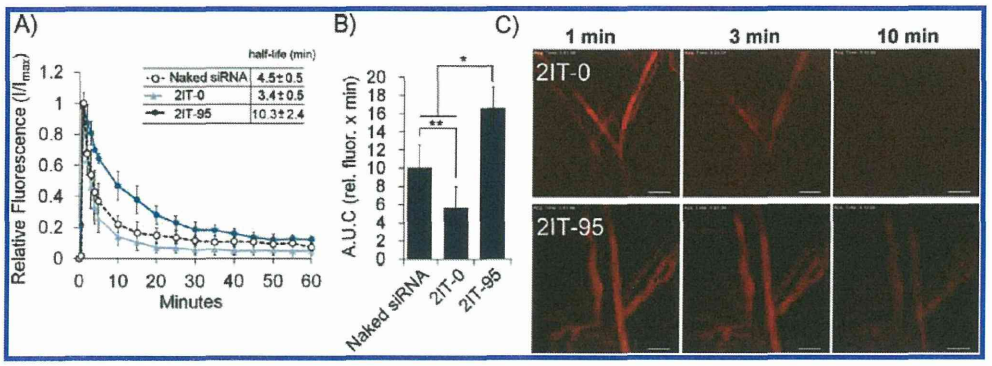

Figure 6. Blood circulation properties of micelles following tail-vein injection (24 μg siRNA). (A) Fluorescence signal over time and calculated half-lives, $n = 3$. (B) Area under the curve values 60 min after injection, $n = 3$, * $p < 0.05$, ** $p = 0.1$. (C) Ear-lobe dermis snap-shots at 1, 3, and 10 min following micelle injection; siRNA fluorescence is shown as red, scale bar = 100 μm.

resulting in broader subcellular distribution in nonlysosomal regions.

It is also interesting to note that internalization of cRGD conjugates may also facilitate their transport into the cell cytoplasm. All nucleic-acid-based therapeutics must gain access to the cytoplasm (and further import into the nucleus for pDNAs) in order to be effective. Due to their large size and highly charged nature, nucleic acids cannot readily diffuse across membranes, whether cell surface, endosomal, or lysosomal in nature. There is building evidence, including the current work, showing that incorporation of cRGD into nucleic acid delivery systems improves their efficacy, even when delivery systems do not contain programmed endosome/lysosome escape functionality.[21,34] In those studies, the nucleic acid cargo associated with the cRGD peptide is shown to have a broader subcellular distribution and in some cases avoids a high degree of colocalization with lysosomal compartments, as was observed in our current study. This could be a characteristic of the internalization route itself; that is, particles are not trafficked to lysosomes, or accumulation in lysosomes is delayed, or that particles escape endocytotic vesicles before or after transport to the lysosome. A previous study regarding the subcellular trafficking of adenovirus vectors showed that RGD motifs at the penton base improved endosomal escape of the virus, even when lysosome acidification was prevented with ammonium chloride (preventing another pH-dependent viral escape mechanism from occurring).[27] Thus, the cRGD peptide may be associated with a natural mechanism that facilitates cytoplasmic entry. Altogether, our data showed that improved cell uptake and broader subcellular distribution was correlated with higher RNAi activity in cultured HeLa-luc cells treated with cRGD-2IT-95 micelles, but the exact mechanism of siRNA cytoplasmic entry remains unclear and needs further investigation. We plan to investigate the subcellular trafficking of siRNA delivered with cRGD-2IT-95 micelles in more detail using blockers of specific cellular internalization pathways (*e.g.*, filipin for caveole pathways, chlorpromazine for clatherin-dependent pathways, and amiloride for macropinocytosis), advanced reagents available for imaging endocytotic vesicles (*e.g.*, CellLite reagents for preparing fluorescent protein-labeled early and late endosomes), and also reagents known to disrupt lysosome structures (*e.g.*, chloroquine).

Blood Stability of Micelles. In order to achieve tumor targeting by IV injection, micelles must remain in the bloodstream long enough to reach the tumor mass. Micelle stability is related to the core structure, and thus the effect of 2IT modification on blood stability was assayed. Blood circulation behavior was determined using intravital real-time confocal laser scanning microscopy (IVRTCLSM) imaging of micelles prepared with fluorescent-labeled siRNA. IVRTCLSM is a non-invasive technique that allows quantification of fluorescence intensity in the ear-lobe dermis of mice and also observation of physical behavior (such as aggregation) of micelles in the bloodstream.[35,36]

Fluorescence intensity curves, calculated half-lives, area under the fluorescence intensity curves (AUCs), and representative ear snap-shots of micelle formulations following injection are shown in Figure 6. Calculation of the circulation half-lives and AUC values showed that micelles prepared with 2IT modified polymer increased the blood residence time of siRNA (Figure 6A,B), demonstrating the importance of micelle stability for improved blood circulation. Specifically, 2IT-95 micelles showed an over 2-fold improvement of circulation half-life and 70% increase in total fluorescence over 60 min compared to naked siRNA. On the other hand, 2IT-0 micelles were quickly and completely removed from the bloodstream, similar to naked siRNA. None of the samples showed aggregation following injection, and fluorescent signal remained homogeneous without visible aggregates throughout the entire observation period (Figure 6C).

Biodistribution of siRNA Administered in Micelle Formulations. Accumulation of siRNA within tumors is critical for effective RNAi-based cancer treatment. The ability of

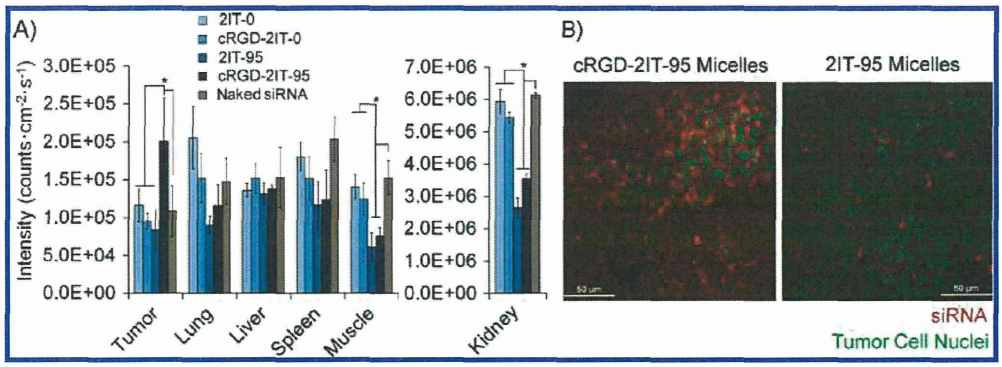

Figure 7. Biodistribution of siRNA administered in micelle formulations 24 h post-injection (24 μg siRNA injected). (A) Quantification of Cy5.5-siRNA fluorescence by IVIS, $n = 4$, $^*p < 0.05$. (B) IVRTCLSM image of H2BGFP-HeLa tumors in live mice 24 h after injection of micelles prepared with Cy5-siRNA (24 μg Cy5-siRNA injected).

micelle formulations to deliver siRNA to subcutaneous HeLa tumors was estimated using IVIS imaging of fluorescent siRNAs 24 h post-injection. This time point was chosen because *in vitro* results revealed that the onset of gene silencing was gradual and thus micelles must accumulate and persist in the tumor tissue for an extended time in order to facilitate siRNA release. Enhanced tumor targeting was achieved for cRGD-2IT-95 micelles, with ~2× accumulation compared to naked siRNA, 2IT-0, and cRGD-2IT-0 formulations (Figure 7A). Furthermore, the cRGD peptide was critical for enhanced tumor accumulation, as 2IT-95 micelles lacking the cRGD peptide showed signal intensities similar to naked siRNA, 2IT-0, and cRGD-2IT-0 formulations. In contrast, cRGD-2IT-0 micelles showed no enhancement of tumor accumulation due to the cRGD peptide, which corroborates well with *in vitro* cell uptake results shown in Figure 4. In addition to increasing tumor accumulation, stable micelles prepared with 2IT modified polymer showed decreased accumulation at off-target sites such as the lung, spleen, muscle, and kidney compared to naked siRNA and 2IT-0 micelles. This demonstrates that stable micelle structures can allow more control of siRNA distribution following injection to favor enhanced accumulation within the target site of activity.

Overall, the highest fluorescence signal for all micelle formulations was found in the kidneys. This is interesting because the kidney filters components present in the bloodstream based on size, and it is generally accepted that the filtration cutoff is on the order of ~5–10 nm.[37] This suggests that 2IT-0 micelles dissociated in the bloodstream, allowing lower molecular structures or free siRNA to enter and accumulate within this blood filtration organ. The fact that 2IT-95 and cRGD-2IT-95 micelles are better at evading kidney accumulation further supports the fact that they form stable structures. On the basis of these findings, it appears that the primary excretion route of the micelles presented here is glomerular filtration, which is an advantage compared to other nanoparticles with prolonged circulation, which often show high liver accumulation. This property could reduce potential side effects such as hepatotoxicity.

Tumor accumulation was also observed using IVRTCLSM imaging of tumors in live mice 24 h post-injection of cRGD-2IT-95 micelles or 2IT-95 micelles, and results were in good agreement with IVIS results. In this experiment, H2BGFP-HeLa cells were used, which allows identification of HeLa cancer cells by the green fluorescent protein (GFP) signal located in the cell nucleus.[38] Fluorescence signal was higher and more broadly distributed for cRGD-2IT-95 micelles containing the cRGD ligand, showing that tumor uptake was improved by the cRGD peptide (Figure 7B). It is also important to note that the fluorescent dye observed is attached to siRNA and not the polymer carrier. Thus, improved tumor accumulation for cRGD-2IT-95 micelles suggests that siRNA is associated with micelle structures at the time of cellular entry. In the current study, only +/− cRGD micelles were compared for tumor-targeting properties and no control peptide with a different amino acid sequence was used. However, specificity of the cRGD sequence has already been demonstrated, as changing the peptide sequence to cRAD abolishes tumor-targeting ability.[39]

The micro distribution of siRNA within HeLa H2BGFP tumors, the region surrounding tumors, and blood vessels distant from tumors were further investigated IVRTCLSM in live mice 24 h after injection of cRGD-2IT-95 or 2IT-95 micelle formulations (Figure 8). Higher fluorescence signal in tumor cells and also enhanced accumulation of siRNA within blood vessels in close proximity (several hundred micrometers) to the tumor mass was observed for cRGD-2IT-95 micelles. Endothelial cells that are activated by tumor growth signals are known to express more integrin receptors that specifically bind to the cRGD peptide.[40] For cRGD-2IT-95 micelles, blood vessels containing fluorescent siRNA were abundant and easy to locate in the region surrounding the tumor mass and in vessels directly entering the tumor. In contrast, blood vessels could not be located in tumors treated with

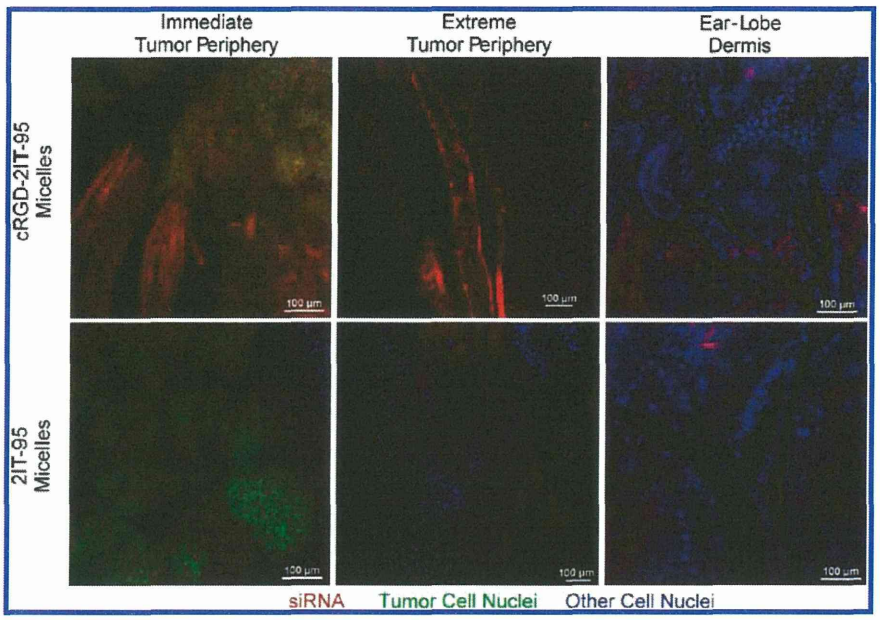

Figure 8. Micro distribution of siRNA 24 h post-injection of micelles. Micelle solutions prepared with Cy-5 siRNA were injected at a dose of 24 μg siRNA. Extreme tumor periphery corresponds to 500–1000 μm outside of the tumor mass.

2IT-95 micelles lacking the cRGD peptide, even after extensive searching. Blood vessel targeting was specific to the tumor region, as blood vessels in the ear-lobe dermis showed no siRNA accumulation. These findings are consistent with another report showing the accumulation of cRGD-containing particles in blood vessels associated with tumors.[41] Altogether, the finding that cRGD-2IT-95 micelles showed enhance accumulation in both the tumor mass and also tumor-associated blood vessels suggests that both sites are accessible targets for therapeutic siRNA treatment.

Therapeutic Activity of siRNA Administered in Micelle Formulations. Polymeric siRNA micelles were evaluated for their ability to suppress the growth of subcutaneous HeLa tumors using an antiangiogenic treatment strategy. Angiogenesis is the process in which new blood vessels are formed within the region of a growing tumor in order to enhance the supply of nutrients to the cancer cells. Vascular endothelial growth factor (VEGF) and vascular endothelial growth factor receptor-2 (VEGFR2) are central to the process of new blood vessel formation in growing tumors, and their effects are reviewed in detail elsewhere.[42,43] VEGF is a protein excreted by tumor cells in order to initiate the angiogenic process, and expression can be up regulated in response to hypoxia in ischemic tissues (*i.e.*, poorly vascularized tumors). VEGFR2 controls the majority of downstream effects of VEGF and is expressed in blood vessel endothelial cells, with expression heightened in the region of growing tumors. Upon activation by VEGF, endothelial cells respond by increasing the microvascular permeability and also show increased proliferation and migration to form new blood vessels.[42]

Antiangiogenic therapy with siRNAs contained in cRGD-functionalized siRNA nanoparticles was first described by Schiffelers *et al.* to inhibit ocular neovascularization as well tumor growth of a N2A murine neuroblastoma cancer model and has since been verified by another group as well.[44–46] Thus, the previous precedent of this strategy for suppression of tumor growth seemed appropriate to confirm the *in vivo* efficacy of our micelle siRNA delivery system. In the above-mentioned studies, siRNAs targeting vascular endothelial growth factor receptors 1 and 2 (VEGFR1 and VEGFR2) were used. We chose to target VEGFR2 and also VEGF itself, in order to disrupt both the transmitting and receiving ends of the angiogenesis signal network. This strategy was chosen following observation of micelle accumulation in both tumor-associated blood vessels as well as the tumor mass. By simply changing the siRNA sequences used the specific target site of siRNA activity can be modulated to target both types of tissue showing siRNA accumulation, VEGFR2 siRNA targets blood vessel endothelial cells while VEGF siRNA targets the tumor mass.

Micelles were prepared incorporating VEGF or VEGFR2 siRNAs in separate micelles. Micelles containing the different siRNA sequences were injected (24 μg siRNA/injection) separately on consecutive days, followed by two days with no injection, and this cycle was repeated three times. The 2 day gap in the injection cycle was chosen based on *in vitro* results that showed gene silencing gradually increased over 50 h, thus a properly timed dosing schedule could potentially prolong the RNAi benefit.

Growth curves of HeLa-luc tumors treated with micelle formulations are shown in Figure 9A. No tumor growth inhibition was observed for naked siRNA,

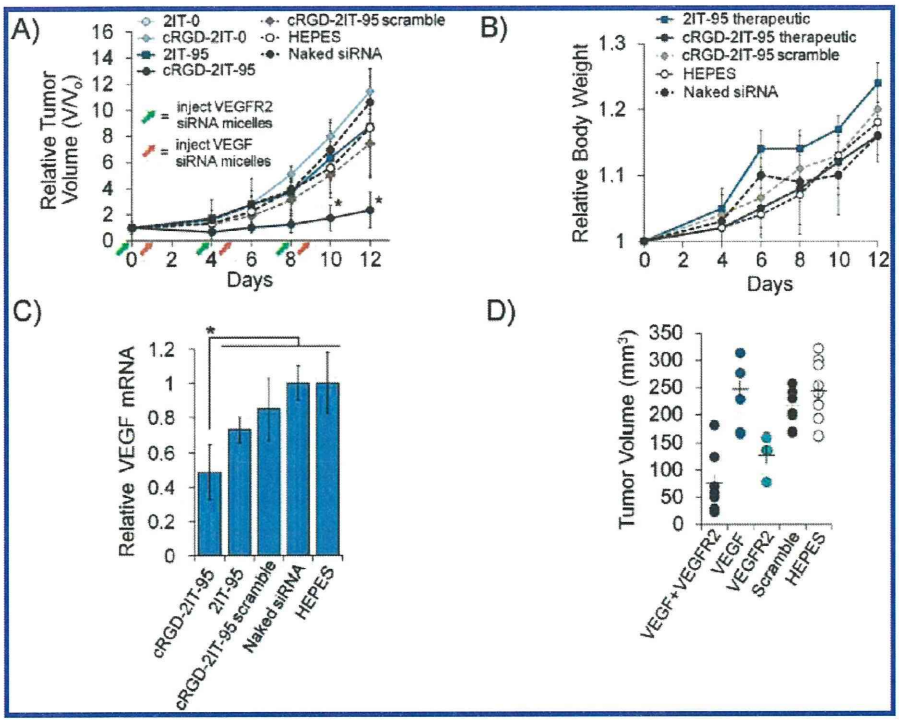

Figure 9. Treatment of subcutaneous HeLa-luc tumors with micelles containing antiangiogenic siRNA. (A) Tumor growth following treatment with micelles containing antiangiogenic siRNA, $n = 4$, * $p < 0.05$ relative to HEPES control tumors. (B) Mouse body weight during micelle treatment. (C) Quantification of VEGF mRNA in tumor tissue following treatment with micelles, $n = 4$, * $p < 0.05$. (D) Size of individual tumors following treatment with cRGD-2IT-95 micelles containing different siRNA sequences (day 12), $n = 4$–8, average tumor size is indicated by cross symbols.

2IT-95 micelles lacking the cRGD peptide, or cRGD-2IT-0 and 2IT-0 formulations. This is consistent with *in vitro* results, which also revealed that these formulations were ineffective at reducing luciferase expression in cultured HeLa-luc cells. In contrast, marked tumor growth inhibition was achieved for cRGD-2IT-95 micelles, which corroborates well with *in vitro* data showing that this formulation exerts RNAi activity (Figure 3A) and also with biodistribution results that demonstrated increased tumor accumulation for this formulation (Figure 7). No therapeutic effect was observed for cRGD-2IT-95 micelles prepared with scramble siRNA, demonstrating that sequence specificity was achieved. Additionally, no significant change in mouse body weight or overall health was noted following treatment with cRGD-2IT-95 micelles despite multiple injections, which suggests that there is no immediate or severe toxicity associated with micelle treatment (Figure 9B). Direct evidence of the RNAi effect in the tumor mass was found following reverse transcription polymerase chain reaction (RT-PCR) analysis of VEGF mRNA levels. The mechanism of siRNA activity results in degradation of target mRNA, which can be quantified by RT-PCR. Thus, this analysis provides molecular proof of the RNAi effect. Tumors treated with cRGD-2IT-95 micelles showed a clear reduction (~50%) of VEGF mRNA levels, whereas tumors treated with 2IT-95 micelles lacking the cRGD peptide were less effective, and cRGD-2IT-95 micelles containing scramble siRNA showed no difference compared to naked siRNA and untreated tumors (Figure 9C). Together, these results confirm that cRGD-2IT-95 micelles can reduce protein expression in the tumor mass by the RNAi mechanism and that the cRGD peptide is critical for maximizing the siRNA activity of this formulation.

Attempts to quantify VEGFR2 mRNA levels in tumors were unsuccessful, as results were inconsistent and contained large errors despite repeated analysis (data not shown). This is likely due to the relatively low number of endothelial cells contained in the excised tumors, making reference to house-keeping genes difficult as a result of inhomogeneous cell populations. As a result, we qualitatively assessed the activity of individual siRNA sequences contained in cRGD-2IT-95 micelles in a different group of mice. Tumor growth inhibition was achieved for micelles containing VEGFR2 siRNAs, confirming that endothelial cell targeting was successful (Figure 9D). Interestingly, tumor growth was not inhibited following treatment with VEGF siRNA alone, although gene silencing was confirmed by RT-PCR experiments. This suggests that partial knockdown of VEGF in HeLa-luc tumors is ineffective to inhibit this fast growing tumor model. Overall, tumors treated with the combination of VEGF and VEGFR2 siRNAs grew the least, probably due to a synergistic effect when both types of siRNAs are used together.

In summary, we have found a multifunctional block copolymer that can be used to form polymeric micelles with siRNA that elicit therapeutic activity toward solid tumors following intravenous injection. Control of the chemistry contained in synthetic block copolymers improved micelle formation with siRNA and also the stability of resulting structures. Nearly complete amine modification of PEG-*b*-PLL with 2IT resulted in a unique and versatile polycation that formed stable micelle structures with siRNA without sensitivity to precise molar ratios of polymer and siRNA. High micelle stability was achieved through a combination of covalent disulfide cross-links in the micelle core and noncovalent interactions due to 2-iminothiolane ring structures in the polymer structure.

The cRGD peptide was crucial for realization of RNAi both *in vitro* and *in vivo*. On the cellular level, this is quite interesting because the cRGD-2IT-95 polymer used for micelle formation in this work does not have designed endosome escape functionality, as evidenced by the lack of activity for micelles without the cRGD peptide. Currently, many siRNA delivery systems are specifically designed to facilitate site-specific release of siRNAs from endosome and lysosome compartments, often exploiting the change in pH following accumulation in these subcellular vesicles. However, delivery efficacy can be improved by utilizing other biological pathways that change the subcellular trafficking and distribution of siRNA. This could prove to be a fundamental new design strategy for next-generation siRNA delivery vehicles that can avoid rapid accumulation in lysosomes.

The combination of improved blood stability and tissue-targeting ability of the cRGD peptide enhanced the accumulation of micelles in both tumor blood vessels and the tumor mass, allowing two tissue types to be utilized for antiangiogenic therapy. Herein lies a distinct advantage of siRNA therapeutics, as disease targets can be expanded by simply changing the nucleotide sequence of siRNA while utilizing the same carrier. This is often not the case for small molecule delivery systems where the chemistry of the carrier is matched with a specific drug (*e.g.*, doxorubicin hydrazone conjugates) and site-specific activity depends on site-specific targeting ability of the carrier. Furthermore, the choice of siRNA sequences is critical for therapeutic benefit to be realized. Here, we found that VEGFR2 was more effective than VEGF for HeLa-luc tumor growth inhibition, although VEGF mRNA knockdown was confirmed.

We will continue to explore ways to expand upon this siRNA delivery platform and increase its efficacy and scope of treatable targets. Modulating the types of siRNA contained in the micelle core can easily be achieved once new target sequences are identified. Additionally, conjugation of different peptides to the polymer could provide specificity for different disease sites or further alter the subcellular trafficking of micelles. The chemistry used to couple the cRGD peptide can be extended to any peptide containing an N-terminal cysteine, thus providing a convenient synthetic handle for polymer conjugation. Development of effective siRNA therapies continues to be a major focus in our lab and in the field of drug delivery. The cRGD-2IT-95 polymeric micelle siRNA delivery system described in this work demonstrates the feasibility of cancer treatment by intravenous injection of therapeutic siRNAs and represents a significant step forward for development of this therapeutic modality toward practical application.

CONCLUSIONS

In this study, we identified a polymeric micelle formulation that is capable of delivering siRNA to solid tumors and exerting a therapeutic benefit by RNAi activity. PEG-*b*-PLL served as the core polymer structure for micelle formation, but modification of lysine amines with 2-iminothiolane was needed for increased stability, and installation of the cRGD peptide on the PEG terminus was necessary for improved biological activity including: RNAi activity, improved cell uptake, and broader subcellular distribution. Stable and targeted micelle structures improved siRNA accumulation within tumors and their associated blood vessels following IV injection, and effective tumor treatment was realized by targeting angiogenic proteins for knockdown at both sites of micelle accumulation. These results demonstrate that polymeric micelles can be used for siRNA cancer therapies administered by intravenous injection.

METHODS

General. *N*-Methyl-2-pyrrolidinone (NMP, 99.5% anhydrous), LiCl (>99%), diisopropylethylamine (DIPEA, 99.5%), 2 N HCl solution, D_2O (99.9%), tetramethylsilane (TMS, 99.5%), and DCl (35% in D_2O) were obtained from Sigma Aldrich (St. Louis, MO) and used without further purification. 2-Iminothiolane hydrochloride (2IT), diethyl ether (99+%), dithiothreitol (DTT, molecular biology grade DNase and RNase free), ethylenediamine tetraacetic acid disodium salt dihydrate (EDTA, 99.5%), sodium dihydrogen phosphate·$2H_2O$ (99−102%), disodium hydrogen phosphate·$12H_2O$ (99+%), glutathione (reduced form), and sodium chloride (99+%) were supplied by Wako Pure Chemical Industries (Osaka, Japan). Ellman's reagent [5,5-dithio-bis-(2-nitrobenzoic acid)] and slide-a-lyzer dialysis cassettes (MWCO = 3.5 kDa) were obtained from Thermo Scientific (Rockford, IL). Sterile HEPES (1 M, pH 7.3) was purchased from Amresco (Solon, OH). Spectra/Por dialysis tubing (6−8 KDa MWCO) was acquired from Spectrum Laboratories (Rancho Dominguez, CA). The cyclo-[RGDfK(C-ε-Acp) peptide (cRGD peptide) was purchased from Peptide Institute Inc., Osaka, Japan.

siRNAs were synthesized by Hokkaido System Science Co., Ltd., and sequences used are as follows: (1) Firefly GL3 luciferase:

5′-CUU ACG CUG AGU ACU UCG AdTdT-3′ (sense), 5′-UCG AAG UAC UCA GCG UAA GdTdT-3 (antisense); (2) scramble: 5′-UUC UCC GAA CGU GUC ACG UdTdT-3′ (sense), 5′-ACG UGA CAC GUU CGG AGA AdTdT-3′ (antisense); (3) VEGF (human): 5′-GGA GUA CCC UGA UGA GAU CdTdT-3′ (sense), 5′-GAU CUC AUC AGG GUA CUC CdTdT-3′ (antisense); (4) VEGFR2 sequence 1 (mouse): 5′-AUG CGG CGG UGG UGA CAG UdTdT-3′ (sense), 5′-ACU GUC ACC ACC GCC GCA UdTdT-3′ (antisense); (5) VEGFR2 sequence 2 (mouse): 5′-AGC UCA GCA CAC AGA AAG AdTdT-3′(sense), 5′-UCU UUC UGU GUG CUG AGC UdTdT-3′ (antisense). Fluorescent firefly GL3 luciferase siRNA contained the fluorophore (Cy3, Cy5, or Cy5.5) attached to the sense strand.

^{1}H NMR analysis of cRGD-PEG-*b*-PLL and 15–45% 2IT modified polymers was conducted in D_2O containing 0.05% v/v tetramethylsilane at 22 °C using a 300 MHz spectrometer (EX 300, JEOL, Tokyo, Japan). cRGD-2IT-95 and 2IT-95 polymers were analyzed in D_2O containing 0.05% v/v tetramethylsilane and 3 μL/mL *DCl solution* (35% *DCl in* D_2O) at 22 °C using a 300 MHz spectrometer (EX 300, JEOL, Tokyo, Japan). Static and dynamic light scattering measurements were performed at 25 °C on a ZetaSizer Nano ZS instrument (Malvern Instruments Ltd., Malvern, UK) equipped with a He–Ne laser (λ = 633 nm) as the incident beam with samples (16 μL) loaded into a Zen 2112 low-volume cuvette. Absorbance and fluorescence measurements were performed with NanoDrop ND-1000 and ND-3300 instruments (NanoDrop Technologies Inc., Rockland, DE), respectively.

The luciferase-expressing human cervical cancer cell line, HeLa-luc, was purchased from Caliper LifeScience (Hopkinton, MA). Dulbecco's modified Eagle's medium (DMEM) was obtained from Sigma Aldrich (St. Louis, MO). Fetal bovine serum was provided by Dainippon Sumitomo Pharma Co. (Osaka, Japan). Falcon Easy-Grip 35 × 10 mm vacuum gas plasma-treated polystyrene tissue culture dishes were obtained from BD Biosciences (San Jose, CA). Luciferin was purchased from Summit Pharmaceutical International (Tokyo, Japan). Luciferase bioluminescence in HeLa-luc cells was measured using an ATTO Kronos Dio photon countable incubator (ATTO Corp., Tokyo, Japan).

All animal experimental procedures were performed in accordance with the Guide for the Care and Use of Laboratory Animals as stated by the National Institutes of Health.

Block Copolymer Synthesis. Acetal-PEG-*b*-PLL block copolymer was synthesized as previously described, comprising a 12 000 MW PEG segment and a 45 amino acid PLL segment, M_w/M_n = 1.2, and all modified polymers were prepared from the same polymer stock.[26] Attachment of cRGD and modification of PLL amines was performed sequentially in aqueous and organic conditions, respectively.

cRGD was coupled to the terminus of acetal-PEG-*b*-PLL by reaction of the N-terminal cysteine contained on cRGD with the aldehyde generated in acetal-PEG-*b*-PLL following incubation at acidic pH. cRGD peptide (26.2 mg, 5 equiv relative to acetal-PEG-*b*-PLL) was dissolved in 1 mL of 10 mM phosphate, pH 7.4, followed by addition dithiothreitol (5 mg, 1 equiv relative to cRGD). The solution was stirred at 25 °C for 30 min to reduce any disulfides present. Acetal-PEG-*b*-PLL (125 mg, 1 equiv) was separately dissolved in 0.2 M sodium acetate buffer, pH 4.0 (5 mL), and then reduced cRGD peptide solution was added dropwise while stirring. The reaction continued for 4 days at 25 °C with continuous stirring. After the reaction period, crude product was transferred to dialysis tubing (SpectraPor, 6–8K MWCO) and dialyzed against 10 mM PBS, pH 7.4, for 2 days, then distilled water for 2 days. Purified cRGD-PEG-*b*-PLL solution was passed through a 0.22 μm filter then frozen and lyophilized. Yield: 112 mg, ~86%, white powder. The amount of cRGD conjugated to the polymer was estimated by ^{1}H NMR, using the integration ratio of phenyl *CH* proton peaks of cRGD to PEG CH_2 backbone peaks. The cRGD introduction rate was typically 70–80%.

2-Iminothiolane modification was achieved by reaction of primary amines in PLL with 2IT according to our previously described method.[15] First, cRGD-PEG-*b*-PLL (55 mg, 0.12 mmol amine, 1 equiv) was added to 5 mL of *N*-methyl pyrrolidinone (NMP) containing 5 wt % LiCl, and the reaction vessel was purged with Ar, capped with a septum, and stirred. The polymer solution was stirred vigorously at 50 °C for 30 min to completely dissolve all solids. Next, diisopropylethylamine (DIEA, 252 μL, 5 equiv relative to lysine amines) was added to the polymer solution under Ar through the septum. 2IT·HCl (106 mg) was separately dissolved in NMP containing 5% LiCl (7.86 mL) and DIEA (134 μL, 1 equiv relative to 2IT) under argon to yield a 96 mM solution. 2IT solution (3 mL, 2.4 equiv relative to Lys amines) was added to the polymer solution dropwise while stirring under Ar atmosphere, and the reaction continued for 18 h at 25 °C. After 18 h, the reaction was terminated by precipitation into a 10-times volume excess of dry diethyl ether. Precipitated product was washed several times with ether and dried under vacuum to a constant mass. Crude product was dissolved in PBS buffer, pH 6.0, and then dialyzed (SpectraPor7, 10 kDa MWCO) against PBS pH 6.0 for 1 day and distilled water for 1 day with frequent media changes. Dialyzed product solution was passed through a 0.2 μM filter and then lyophilized. Yield: 61 mg (~85%), white powder. The degree of IM introduction was determined from the ^{1}H NMR spectrum by the peak intensity ratio of the β, γ, δ-methylene protons of Lys ($(CH_2)_3$, δ = 1.3–1.9 ppm) to the protons of trimethylene units of mercaptopropyl groups (HS-$(CH_2)_3$, δ = 2.1–2.8 ppm). The calculated 2IT introduction rate was ~95%. The cRGD content of polymers did not change following the 2IT modification procedure.

Analysis of Thiol Content. Polymer solutions (5 mg/mL) were incubated in 10 mM HEPES buffer containing 5 mM EDTA and 15 mM DTT for 30 min at room temperature to reduce any disulfides present. The reduced polymer solution was placed on ice and handled in a timely manner at 0–4 °C until the addition of Ellman's reagent.[47] After reduction, DTT was removed from the polymer solution using a NanoSep centrifugation device (3000 MWCO). Samples were subjected to three successive concentration/rinsing cycles with 10 mM HEPES containing 5 mM EDTA as the rinsing buffer. After the final centrifugation cycle, concentrated polymer solution was collected and diluted to its original volume. The final flow-through fraction was also collected and diluted in the same manner as the polymer-containing fraction to determine the amount of DTT remaining in the sample. Polymer and flow-through samples were subjected to Ellman's assay according to the manufacturer's protocol, and sample absorbance was measured at 412 nm. Free thiol content of solutions were determined from a standard curve generated with reduced glutathione. Polymer thiol content was obtained by subtracting the thiol content in the flow-through fraction to correct for residual DTT. PEG-*b*-PLL was analyzed as a negative control in a similar fashion, except the polymer solution (5 mg/mL) was used directly without DTT incubation. Thiol content in cross-linked micelles was determined similarly as described above, except that micelle solutions were added directly to Ellman's reagent solution without additional treatment as described for polymer samples.

Micelle Preparation. Polymer samples were dissolved in 10 mM HEPES buffer (pH 7.4) at a concentration of 5 mg/mL. For cRGD-2IT-0 and 2IT-0 micelles, polymer stock solution was further diluted to the polymer/siRNA molar ratio of 1.2 and mixed with siRNA solution (15 μM in HEPES, pH 7.4). The solution was vortexed briefly to yield micelles. For cRGD-2IT-95 and 2IT-95 micelles, DTT was added (30 mg/mL) to polymer stock solution, and the polymer was incubated for 30 min at room temperature to cleave any disulfides present. After DTT reduction, polymer solution was added to siRNA solution (15 μM in HEPES, pH 7.4) and the mixture was vortexed. Micelle solution was then transferred to a slide-a-lyzer cassette (MWCO = 3.5 kDa) and dialyzed against HEPES (pH 7.4) containing 0.5% DMSO for 2 days, followed by dialysis against HEPES (pH 7.4) for 2 days. Micelles were recovered from the slide-a-lyzer cassette and passed through a 0.2 μm filter before use.

Micelle Characterization. Micelles were analyzed by static and dynamic light scattering (DLS) to determine scattered light intensity (SLI) and size/PDI, respectively. Size distributions were determined by cumulant and histogram analysis of DLS data using the software provided by the manufacturer. Results are shown as the *z*-average diameter (cumulant mean) with the polydispersity index (PDI) (defined in the ISO standard

document 13321:1996) and histogram of size distribution. The ζ-potentials of micelles were measured by laser Doppler electrophoresis in 10 mM HEPES buffer (pH 7.4) containing 150 mM NaCl at 37 °C. All samples were equilibrated to the defined temperature for 2 h prior to measurement. Atomic force microscopy (AFM) imaging of the siRNA complexes was carried out in air using a Bruker AXS MMAFM Nanoscope V (Madison, WI) operated by Scan Assist with a standard silicon probe on the freshly cleaved mica substrate. Raw AFM images were processed by flattening to remove the background slope of the substrate surface.

***In Vitro* Micelle Stability.** Micelle stability was measured in the presence of 150 and 600 mM NaCl in the presence or absence of the disulfide reducing agent DTT. Micelle samples were diluted 1:1 with NaCl solution at desired concentrations and incubated at 37 °C for 24 h. Samples subjected to disulfide reducing conditions were diluted in the same fashion as above, however, with NaCl solutions containing 200 mM DTT. After the 24 h incubation period, samples were measured by static and dynamic light scattering as described in the micelle characterization section. Relative micelle stability was determined by dividing the scattered light intensity of treated samples with the scattered light intensity of samples diluted in the same fashion with only HEPES buffer.

***In Vitro* Gene Silencing.** HeLa human cervical cancer cells stably expressing luciferase (HeLa-luc) were seeded onto 35 mm Petri dishes (25 000 cells/dish) and allowed to attach for 24 h. After cell attachment, the medium was removed and replaced with media (2 mL) containing 100 μM luciferin and cross-linked micelles (200 nM siRNA). For each analysis, control samples were prepared by addition of media diluted with HEPES instead of micelle solution. The total dilution of media after addition of luciferin and micelle solution was less than 200 μL additives per 10 mL of media. Samples were placed into a Kronos real-time photon countable incubator, and the luminescence intensity was measured periodically over a 50 h time period, with the temperature and CO_2 maintained at 37 °C and 5%. Relative luminescence was determined by dividing the average luminescence intensity of treated samples by the average luminescence intensity of control samples, $n = 4$. Cells were cultured in Dulbecco's modified Eagle's medium (DMEM) containing 10% fetal bovine serum (FBS) and antiobiotics during the experiment.

Cytotoxicity. HeLa-luc cells were seeded onto 24-well plates (10 000 cells/well) and allowed to attach for 24 h under standard cell culture conditions. Next, the medium was removed and replaced with fresh media supplemented with cross-linked micelles at the desired siRNA concentration. Cells were further incubated with micelle-containing media for 48 h. Metabolism was assessed following 1 h incubation with cell counting kit 8 solution (1 μL/10 μL media) (CCK 8, Dojindo Laboratories, Kumamoto, Japan) followed by absorbance measurement of extracellular media at 450 nm. All data are expressed relative to untreated control cells, $n = 6$.

Cell Uptake. HeLa-luc cells were seeded onto 6-well plates (100 000 cells/well) and allowed to attach for 24 h. After the attachment period, medium was exchanged with fresh media containing micelles prepared with Cy3-siRNA (300 nM). Cells were incubated with micelle-containing media for 2 h under standard cell culture conditions then rinsed four times with PBS and harvested by trypsinization. Harvested cells were subjected to flow cytometric analysis using a BD LSR II instrument (BD Biosciences, San Jose, CA) equipped with appropriate excitation/emission filter combinations, and forward and side-scatter gates were set to exclude debris. A total of 10 000 events were recorded for each analysis, and data were analyzed using BD FACSDiva software (BD Biosciences).

***In Vitro* Confocal Microscopy.** HeLa-luc cells (50 000 cells) were seeded onto a 35 mm glass bottom dish (Iwaki, Tokyo, Japan) and allowed to attach for 24 h. Micelles were prepared with Cy5 siRNA (2IT-95) or Cy3 siRNA (cRGD-2IT-95) and introduced simultaneously to cells (500 nM siRNA each) followed by incubation for 4 h. After incubation with micelles, the medium was exchanged with fresh media containing LysoTracker Green (Invitrogen Molecular Probes, Eugene OR) and Hoechst 33342 (Dojindo Laboratories, Kumamoto, Japan), and the cells were incubated for an additional 15 min. Cells were rinsed with PBS containing Ca^{2+} and Mg^{2+} and imaged in this buffer. Confocal laser scanning microscopy was performed in live cells using a LSM 510 (Carl Zeiss, Oberlochen, Germany) with a C-Apochromat 63× objective (Carl Zeiss) and appropriate excitation sources and emission filters. Data were analyzed using LSM imaging software (Carl Zeiss). Colocalization was determined with respect to Cy3, Cy5, and LysoTracker using the following equation: relative colocalization = $\Sigma pixels_{colocalized}/\Sigma pixels_{total}$.

Blood Circulation. Micelle stability in the blood compartment was evaluated using intravital confocal laser scanning microscopy (IVRTCLSM) in live mice. All picture/movie acquisitions were performed using a Nikon A1R confocal laser scanning microscope system attached to an upright ECLIPSE FN1 (Nikon Corp., Tokyo, Japan) equipped with a 20× objective, 640 nm diode laser, and a band-pass emission filter of 700/75 nm. The pinhole diameter was set to result in a 10 μm optical slice. Eight-week-old female BALB/c nude mice (Oriental Yeast Co., Ltd., Tokyo, Japan) were anesthetized with 2.0−3.0% isoflurane (Abbott Japan Co., Ltd., Tokyo, Japan) using a Univenter 400 anaesthesia unit (Univentor Ltd., Zejtun, Malta). Mice were then subjected to lateral tail vein catheterization with a 30 gauge needle (Dentronics Co., Ltd., Tokyo, Japan) connected to a nontoxic, medical grade polyethylene tube (Natsume Seisakusho Co., Ltd., Tokyo, Japan). Anesthetized mice were placed onto a temperature-controlled pad (Thermoplate; Tokai Hit Co., Ltd., Shizuoka, Japan) integrated into the microscope stage and maintained in a sedated state throughout the measurement. Ear-lobe dermis was observed without surgery following fixation beneath a coverslip with a single drop of immersion oil. Data were acquired in video mode for 3 min (30 frames/s), followed by snap-shots every 1 min thereafter. All animal experimental procedures were performed in accordance with the Guide for the Care and Use of Laboratory Animals as stated by the National Institutes of Health.

Micelles prepared with Cy5-labeled siRNA were injected (200 μL of 9.2 μM siRNA, ~24 μg total siRNA) *via* the tail vein 10 s after the start of video capture. Video data were analyzed by selecting regions of interest (ROIs) within blood vessels or extravascular skin tissue, and the average fluorescence intensity per pixel for each time point was determined using the Nikon NIS-Elements C software provided by the manufacturer. To produce the blood retention profiles shown in Figure 6, vein fluorescence data were expressed relative to the maximum observed value (typically 45 s to 1 min.). First, the background fluorescence intensity was determined from video captured during the 10 s before sample injection. This background value was subtracted from the average pixel intensities measured after micelle injection to create background-corrected intensities for each time point. Next, relative fluorescence intensities were determined by dividing the average fluorescence intensity at each time point by the maximum observed fluorescence intensity. Each experiment was performed in triplicate in separate animals. A detailed description of the microscope apparatus and mouse positioning for IVRTCLSM, as well as examples of data workup showing ROIs, can be found in our previously published report.[35] Half-lives were calculated by plotting the natural log of intensity *versus* time for the initial period of signal decay (10 min for naked siRNA and 2IT-0, 15 min for 2IT-95). The slope of these plots were determined and applied to the half-life equation: $T_{1/2} = 0.693/(-\text{slope})$. Areas under the curve values were calculated using the trapezoid rule.

Biodistribution. HeLa-luc tumors were prepared by *in vivo* passage of solid tumor fragments. Donor tumors were prepared by injecting HeLa-luc cells (2.6×10^6 cells) under the skin in the right rear flank of BALB/c nude mice and allowed to mature for 2 weeks. After 2 weeks, donor tumors were excised and cut into 3 × 3 mm pieces. Tumor fragments were transplanted under the skin into the rear flank of 6 week old female BALB/c nude mice, and the wound was closed with a suture. Tumors were allowed to mature for 8 days, then mice were randomly assigned into treatment groups ($n = 4$ per group). Mice were fed alfalpha-free chow for 2 weeks before injecting micelle samples. Micelles prepared with Cy5.5 siRNA were injected (200 μL of 9.2 μM siRNA, ~24 μg total siRNA) *via* the tail vein.

After 24 h, mice were sacrificed and individual organs were excised and rinsed with PBS. Organs and tumors were imaged using an IVIS instrument in fluorescence mode with appropriate excitation and emission filters. Data were analyzed using Living Image software by drawing ROIs around whole organs to determine the total photon counts and signal area in square centimeters. The fluorescence intensity was normalized to sample area and irradiation time using the following equation: intensity = total photons/[illumination time (s) × area (cm^2)].

***In Vivo* Confocal Microscopy.** Micelles prepared with Cy5 siRNA were injected (200 μL of 9.2 μM siRNA, ~24 μg total siRNA) *via* the tail vein into mice bearing subcutaneous HeLa-H2BGFP tumors. HeLa-H2BGFP cells express green fluorescent protein (GFP) in the cell nucleus, which allows identification of tumor cells. After 24 h, mice were anesthetized and Hoechst 33342 dye (8 mg/kg in PBS, Lonza Group Ltd., Basel, Switzerland) was used to stain the nuclei of cells present in circulation and the perivascular space. Next, the tumor was exposed by a series of dorsal cuts in the skin surrounding the tumor to create a hinged skin flap with the tumor attached to the skin, while leaving blood vessels feeding the tumor intact. The exposed tumor was mounted under a coverslip and imaged using the IVRTCLSM equipped with a 40 or 60× objective. Hoechst, GFP, and Cy5 signals were detected simultaneously using 405, 488, and 640 nm excitation lasers and band-pass emission filters of 450/50, 525/50, and 700/75 nm, respectively. Images were analyzed using the Nikon NIS-Elements C software provided by the manufacturer.

Tumor Growth Inhibition. HeLa-luc tumors were prepared by *in vivo* passage of solid tumor fragments. Donor tumors were prepared by injecting HeLa-luc cells (2.6×10^6 cells) under the skin in the right rear flank of mice and allowed to mature for 2 weeks. After 2 weeks, donor tumors were excised and cut into 3 × 3 mm pieces. Tumor fragments were transplanted under the skin into the rear flank of 6 week old female BALB/c nude mice, and the wound was closed with a suture. Tumors were allowed to mature for 4 days, then mice were randomly assigned into treatment groups ($n = 4$ per group).

Micelle formulations were screened for *in vivo* efficacy using a combination therapy of VEGFR2 and VEGF siRNAs. Micelles were prepared to contain either type of siRNA in different micelle formulations and were injected separately. Micelle treatment began on day four following tumor implantation. Micelles containing VEGFR2 siRNA were injected on the first day of treatment, micelles incorporating VEGF siRNA were injected on day two, followed by two days with no injection. This sequence was repeated three times for a total of three injections of each micelle formulation and six total injections of micelles. For each injection, 200 μL of micelle solution (9.2 μM siRNA, ~24 μg total siRNA) was administered. The negative control sample for cRGD-2IT-95 formulation was prepared with scramble siRNA and was administered in the same fashion as described above. Tumor size was monitored over time by caliper measurement, and tumor volumes were calculated using the following equation: volume = $^1/_2 a \times b^2$, where a is the long axis and b is the short axis measured.

For determining the effect of each siRNA sequence individually (delivered by cRGD-2IT-95 micelles), subcutaneous tumors were prepared by *in vivo* passage as described above and the injection sequence used was the same, except for samples delivering only one type of siRNA. For groups receiving only one type of siRNA (VEGF or VEGFR2), micelles containing scramble siRNA were injected on the second day to keep the total amount of siRNA micelles injected into each mouse constant. Each group consisted of four mice, with additional data from other groups (HEPES, scramble, and VEGF+VEGFR2 treatment) combined in Figure 9.

PCR Analysis. Tumors were excised from mice 72 h after the last injection of micelles, and ~20 mg of non-necrotic tissue was selected from the tumor mass ($n = 4$ tumors, each tumor was analyzed in triplicate). Tumor fragments were sonicated for 10 s in lysis buffer and then centrifuged to remove excess debris. RNA was extracted from the supernatant using a RNeasy Mini Kit (Qiagen, Valencia, CA) according to the manufacturer's instructions. Extracted RNA samples were normalized to the same 260 nm absorbance value, and genomic DNA was eliminated, followed by RNA transcription to cDNA using a QuantiTect reverse transcription kit (Qiagen, Valencia, CA). RNA was quantified following conversion to cDNA and amplified using real-time PCR. Primers used for human actin and human VEGF were synthesized by Hokkaido System Science (Hokkaido, Japan), and the sequences used were as follows: CCAACCGCGAGAAGATGA (actin forward); CCAGAGGCGTACAGGGATAG (actin reverse); AGTGGTCCCAGGCTGCAC (VEGF forward); TCCATGAACTTCACCACTTCGT (VEGF reverse).

Statistical Analysis. All data are expressed as the average value ± the standard deviation. The p values were determined by the Student's t test using a two-tailed distribution and two-sample unequal variance with the T.Test function of Microsoft Excel. The p values of less than 0.05 were considered as statistically significant.

Conflict of Interest: The authors declare no competing financial interest.

Acknowledgment. This research was financially supported by the Funding Program for World-Leading Innovative R&D in Science and Technology (FIRST), and the Core Research Program for Evolutional Science and Technology (CREST) from the Japan Science and Technology Agency (JST). Additional support was provided to R.J.C. by the Japan Society for the Promotion of Science postdoctoral fellowship program. We thank T. Kanda (Aichi Cancer Center Research Institute) for HeLa H2B-GFP cells.

Supporting Information Available: Light scattering intensity of polymer and siRNA mixtures at different molar ratios, and stability of cRGD-2IT-95 and 2IT-95 micelles at 600 mM NaCl is provided. This material is available free of charge *via* the Internet at http://pubs.acs.org.

REFERENCES AND NOTES

1. Fire, A.; Xu, S.; Montgomery, M.; Kostas, S.; Driver, S.; Mello, C. Potent and Specific Genetic Interference by Double-Stranded RNA in *Caenorhabditis elegans*. *Nature* **1998**, *391*, 806–811.
2. Carthew, R.; Sontheimer, E. Origins and Mechanisms of miRNAs and siRNAs. *Cell* **2009**, *136*, 642–655.
3. Judge, A.; MacLachlan, I. Overcoming the Innate Immune Response to Small Interfering RNA. *Hum. Gene Ther.* **2008**, *19*, 111–124.
4. Robbins, M.; Judge, A.; MacLachlan, I. siRNA and Innate Immunity. *Oligonucleotides* **2009**, *19*, 89–101.
5. Turner, J.; Jones, S.; Moschos, S.; Lindsay, M.; Gait, M. MALDI-TOF Mass Spectral Analysis of siRNA Degradation in Serum Confirms an RNAse A-like Activity. *Mol. Biosyst.* **2007**, *3*, 43–50.
6. van de Water, F.; Boerman, O.; Wouterse, A.; Peters, J.; Russel, F.; Masereeuw, R. Intravenously Administered Short Interfering RNA Accumulates in the Kidney and Selectively Suppresses Gene Function in Renal Proximal Tubules. *Drug Metab. Dispos.* **2006**, *34*, 1393–1397.
7. Gary, D.; Puri, N.; Won, Y. Polymer-Based siRNA delivery: Perspectives on the Fundamental and Phenomenological Distinctions from Polymer-Based DNA Delivery. *J. Controlled Release* **2007**, *121*, 64–73.
8. Whitehead, K.; Langer, R.; Anderson, D. Knocking Down Barriers: Advances in siRNA Delivery. *Nat. Rev. Drug Discovery* **2009**, *8*, 129–138.
9. Xie, F.; Woodle, M.; Lu, P. Harnessing *In Vivo* siRNA Delivery for Drug Discovery and Therapeutic Development. *Drug Discovery Today* **2006**, *11*, 67–73.
10. Li, C.; Parker, A.; Menocal, E.; Xiang, S.; Borodyansky, L.; Fruehauf, J. Delivery of RNA Interference. *Cell Cycle* **2006**, *5*, 2103–2109.
11. Gao, K.; Huang, L. Nonviral Methods for siRNA Delivery. *Mol. Pharmaceutics* **2009**, *6*, 651–658.
12. Howard, K. Delivery of RNA Interference Therapeutics Using Polycation-Based Nanoparticles. *Adv. Drug Delivery Rev.* **2009**, *61*, 710–720.
13. Tan, S.; Kiatwuthinon, P.; Roh, Y.; Kahn, J.; Luo, D. Engineering Nanocarriers for siRNA Delivery. *Small* **2011**, *7*, 841–856.

14. Castanotto, D.; Rossi, J. The Promises and Pitfalls of RNA-Interference-Based Therapeutics. *Nature* **2009**, *457*, 426–433.
15. Matsumoto, S.; Christie, R. J.; Nishiyama, N.; Miyata, K.; Ishii, A.; Oba, M.; Koyama, H.; Yamasaki, Y.; Kataoka, K. Environment-Responsive Block Copolymer Micelles with a Disulfide Cross-Linked Core for Enhanced siRNA Delivery. *Biomacromolecules* **2009**, *10*, 119–127.
16. Christie, R.; Miyata, K.; Matsumoto, Y.; Nomoto, T.; Menasco, D.; Lai, T.; Pennisi, M.; Osada, K.; Fukushima, S.; Nishiyama, N.; Yamasaki, Y.; Kataoka, K. Effect of Polymer Structure on Micelles Formed between siRNA and Cationic Block Copolymer Comprising Thiols and Amidines. *Biomacromolecules* **2011**, *12*, 3174–3185.
17. Ruoslahti, E. RGD and Recognition Sequences for Integrins. *Annu. Rev. Cell Dev. Biol.* **1996**, *12*, 697–715.
18. Xiong, J.; Stehle, T.; Zhang, R.; Joachimiak, A.; Frech, M.; Goodman, S.; Arnaout, M. Crystal Structure of the Extracellular Segment of Integrin $\alpha_v\beta_3$ in Complex with an Arg-Gly-Asp Ligand. *Science* **2002**, *296*, 151–155.
19. Haubner, R.; Gratias, R.; Diefenbach, B.; Goodman, S.; Jonczyk, A.; Kessler, H. Structural and Functional Aspects of RGD-Containing Cyclic Pentapeptides as Highly Potent and Selective Integrin $\alpha_v\beta_3$ Antagonists. *J. Am. Chem. Soc.* **1996**, *118*, 7461–7472.
20. Gladson, C. Expression of Integrin $\alpha_v\beta_3$ in Small Blood Vessels of Glioblastoma Tumors. *J. Neuropath. Exp. Neur.* **1996**, *55*, 1143–1149.
21. Oba, M.; Aoyagi, K.; Miyata, K.; Matsumoto, Y.; Itaka, K.; Nishiyama, N.; Yarnasaki, Y.; Koyama, H.; Kataoka, K. Polyplex Micelles with Cyclic RGD Peptide Ligands and Disulfide Cross-Links Directing to the Enhanced Transfection *via* Controlled Intracellular Trafficking. *Mol. Pharmaceutics* **2008**, *5*, 1080–1092.
22. Meister, A.; Anderson, M. Glutathione. *Annu. Rev. Biochem.* **1983**, *52*, 711–760.
23. Singh, R.; Kats, L.; Blattler, W.; Lambert, J. Formation of N-Substituted 2-Iminothiolanes when Amino Groups in Proteins and Peptides are Modified by 2-Iminothiolane. *Anal. Biochem.* **1996**, *236*, 114–125.
24. Tam, J.; Wu, C.; Liu, W.; Zhang, J. Disulfide Bond Formation in Peptides by Dimethyl Sulfoxide—Scope and Applications. *J. Am. Chem. Soc.* **1991**, *113*, 6657–6662.
25. Kenausis, G.; Voros, J.; Elbert, D.; Huang, N.; Hofer, R.; Ruiz-Taylor, L.; Textor, M.; Hubbell, J.; Spencer, N. Poly(L-lysine)-*g*-Poly(ethylene glycol) Layers on Metal Oxide Surfaces: Attachment Mechanism and Effects of Polymer Architecture on Resistance to Protein Adsorption. *J. Phys. Chem. B* **2000**, *104*, 3298–3309.
26. Oba, M.; Fukushima, S.; Kanayama, N.; Aoyagi, K.; Nishiyama, N.; Koyama, H.; Kataoka, K. Cyclic RGD Peptide-Conjugated Polyplex Micelles as a Targetable Gene Delivery System Directed to Cells Possessing $\alpha_v\beta_3$ and $\alpha_v\beta_5$ Integrins. *Bioconjugate Chem.* **2007**, *18*, 1415–1423.
27. Shayakhmetov, D.; Eberly, A.; Li, Z.; Lieber, A. Deletion of Penton RGD Motifs Affects the Efficiency of Both the Internalization and the Endosorne Escape of Viral Particles Containing Adenovirus Serotype 5 or 35 Fiber Knobs. *J. Virol.* **2005**, *79*, 1053–1061.
28. Lu, J.; Langer, R.; Chen, J. A Novel Mechanism Is Involved in Cationic Lipid-Mediated Functional siRNA Delivery. *Mol. Pharmaceutics* **2009**, *6*, 763–771.
29. Dijkgraaf, I.; Kruijtzer, J.; Liu, S.; Soede, A.; Oyen, W.; Corstens, F.; Liskamp, R.; Boerman, O. Improved Targeting of the $\alpha_v\beta_3$ Integrin by Multimerisation of RGD Peptides. *Eur. J. Nucl. Med. Mol. I* **2007**, *34*, 267–273.
30. Liu, S. Radiolabeled Cyclic RGD Peptides as Integrin $\alpha_v\beta_3$-Targeted Radiotracers: Maximizing Binding Affinity *via* Bivalency. *Bioconjugate Chem.* **2009**, *20*, 2199–2213.
31. Sancey, L.; Garanger, E.; Foillard, S.; Schoehn, G.; Hurbin, A.; Albiges-Rizo, C.; Boturyn, D.; Souchier, C.; Grichine, A.; Dumy, P.; Coll, J. Clustering and Internalization of Integrin $\alpha_v\beta_3$ with a Tetrameric RGD-Synthetic Peptide. *Mol. Ther.* **2009**, *17*, 837–843.
32. Wangler, C.; Maschauer, S.; Prante, O.; Schafer, M.; Schirrmacher, R.; Bartenstein, P.; Eisenhut, M.; Wangler, B. Multimerization of cRGD Peptides by Click Chemistry: Synthetic Strategies, Chemical Limitations, and Influence on Biological Properties. *ChemBioChem* **2010**, *11*, 2168–2181.
33. Wattiaux, R.; Laurent, N.; Wattiaux-De Coninck, S.; Jadot, M. Endosomes, Lysosomes: Their Implication in Gene Transfer. *Adv. Drug Delivery Rev.* **2000**, *41*, 201–8.
34. Alam, M.; Ming, X.; Fisher, M.; Lackey, J.; Rajeev, K.; Manoharan, M.; Juliano, R. Multivalent Cyclic RGD Conjugates for Targeted Delivery of Small Interfering RNA. *Bioconjugate Chem.* **2011**, *22*, 1673–1681.
35. Matsumoto, Y.; Nomoto, T.; Cabral, H.; Matsumoto, Y.; Watanabe, S.; Christie, R. J.; Miyata, K.; Oba, M.; Ogura, T.; Yamasaki, Y.; *et al.* Direct and Instantaneous Observation of Intravenously Injected Substances Using Intravital Confocal Micro-Videography. *Biomed. Opt. Express* **2010**, *1*, 1209–1216.
36. Nomoto, T.; Matsumoto, Y.; Miyata, K.; Oba, M.; Fukushima, S.; Nishiyama, N.; Yamasoba, T.; Kataoka, K. *In Situ* Quantitative Monitoring of Polyplexes and Polyplex Micelles in the Blood Circulation Using Intravital Real-Time Confocal Laser Scanning Microscopy. *J. Controlled Release* **2011**, *151*, 104–109.
37. Choi, H.; Liu, W.; Misra, P.; Tanaka, E.; Zimmer, J.; Ipe, B.; Bawendi, M.; Frangioni, J. Renal Clearance of Quantum Dots. *Nat. Biotechnol.* **2007**, *25*, 1165–1170.
38. Kanda, T.; Sullivan, K.; Wahl, G. Histone-GFP Fusion Protein Enables Sensitive Analysis of Chromosome Dynamics in Living Mammalian Cells. *Curr. Biol.* **1998**, *8*, 377–385.
39. Jin, Z.; Josserand, V.; Foillard, S.; Boturyn, D.; Dumy, P.; Favrot, M.; Coll, J. *In Vivo* Optical Imaging of Integrin $\alpha_v\beta_3$ in Mice Using Multivalent or Monovalent cRGD Targeting Vectors. *Mol. Cancer* **2007**, *6*, 41.
40. Eliceiri, B.; Cheresh, D. The Role of α_v Integrins During Angiogenesis: Insights into Potential Mechanisms of Action and Clinical Development. *J. Clin. Invest.* **1999**, *103*, 1227–1230.
41. Montet, X.; Montet-Abou, K.; Reynolds, F.; Weissleder, R.; Josephson, L. Nanoparticle Imaging of Integrins on Tumor Cells. *Neoplasia* **2006**, *8*, 214–222.
42. Hicklin, D.; Ellis, L. Role of the Vascular Endothelial Growth Factor Pathway in Tumor Growth and Angiogenesis. *J. Clin. Oncol.* **2005**, *23*, 1011–1027.
43. Bergers, G.; Benjamin, L. Tumorigenesis and the Angiogenic Switch. *Nat. Rev. Cancer* **2003**, *3*, 401–410.
44. Schiffelers, R.; Ansari, A.; Xu, J.; Zhou, Q.; Tang, Q.; Storm, G.; Molema, G.; Lu, P.; Scaria, P.; Woodle, M. Cancer siRNA Therapy by Tumor Selective Delivery with Ligand-Targeted Sterically Stabilized Nanoparticle. *Nucleic Acids Res.* **2004**, *32*, e149.
45. Kim, B.; Tang, Q.; Biswas, P.; Xu, J.; Schiffelers, R.; Xie, F.; Ansari, A.; Scaria, P.; Woodle, M.; Lu, P.; Rouse, B. Inhibition of Ocular Angiogenesis by siRNA Targeting Vascular Endothelial Growth Factor Pathway Genes - Therapeutic Strategy for Herpetic Stromal Keratitis. *Am. J. Pathol.* **2004**, *165*, 2177–2185.
46. Kim, J.; Kim, S.; Kim, W. PEI-*g*-PEG-RGD/Small Interference RNA Polyplex-Mediated Silencing of Vascular Endothelial Growth Factor Receptor and Its Potential as an Anti-Angiogenic Tumor Therapeutic Strategy. *Oligonucleotides* **2011**, *21*, 101–107.
47. Ellman, G. Tissue Sulfhydryl Groups. *Arch. Biochem. Biophys.* **1959**, *82*, 70–77.